

# Femtosecond stimulated Raman spectroscopy of methanol and acetone in a noncollinear geometry using a supercontinuum probe

Mateusz Plewicki and Robert Levis\*

Department of Chemistry, Center for Advanced Photonics Research, Temple University,  
Philadelphia, Pennsylvania 19122, USA

\*Corresponding author: rjlevis@temple.edu

Received April 9, 2008; revised August 1, 2008; accepted August 5, 2008;  
posted August 13, 2008 (Doc. ID 94831); published September 25, 2008

The design of a femtosecond stimulated Raman spectroscopy (FSRS) setup capable of recording high contrast Raman spectra is presented. The Raman transition is stimulated by a supercontinuum pulse and pumped by the second-harmonic of a Ti:sapphire amplifier system fundamental wavelength. This scheme alleviates rapid amplitude modulation near 800 nm using the smooth amplitude region in the continuum near the 400 nm pump. Raman spectra of acetone and methanol are presented in which the Raman peak intensity is the most pronounced feature of the spectrum. A mechanism limiting the resolution and peak intensity based on the non-linear index of refraction effects is suggested. © 2008 Optical Society of America

OCIS codes: 190.5650, 190.3270, 190.3237, 190.5890.

## 1. INTRODUCTION

We have developed a variant of femtosecond stimulated Raman spectroscopy (FSRS) that has high contrast for vibrational spectroscopy. Vibrational spectroscopy offers the advantages of discrimination and nondestructive identification of molecular samples [1–4]. The latter feature is especially useful when dealing with explosives and other hazardous materials [5]. The high discrimination comes from the characteristic vibrational “fingerprint” of a molecule. Vibrational spectroscopy, however, presents the challenge of measuring absorption in a frequency range spanning from  $50\text{ cm}^{-1}$  to  $3000\text{ cm}^{-1}$ . One solution to this problem is to take advantage of the Raman process [6,7] shown in Fig. 1. This approach has been shown to give satisfactory results in many systems including minerals [8,9], organics [8], benzene [10], and hydrocarbons [11]. The detection of high explosives [5,11] is a current challenge for optical detection. Single-pulse, remote Raman detection is typically based on spontaneous Raman scattering along with the fundamental wavelength. Optically, this is a very simple method, but as the emitted spontaneous Raman is very weak, the signal-to-noise ratios limit applicability. Promising enhancement of the signal has been reported by using shaped femtosecond pulses [12–16] incident upon a methanol sample. The measurement in that experiment focuses, however, on enhancing a single transition in a system that is known, not on obtaining the fingerprint spectrum of multiple unknown species.

A promising method for stand-off detection is stimulated Raman scattering. In this experiment, a photon  $\omega_p$  is converted to lower energy in the case of Stokes scattering or higher energy in the case of anti-Stokes scattering. This occurs through a stimulated process by having both the  $\omega_p$  and the seed Stokes  $\omega_s$  or the anti-Stokes fields  $\omega_A$  coherently interact with the sample, as shown in Fig 1.

To describe the processes under consideration, we first consider differential equations governing Raman gain. The photon occupational numbers for the Raman scattering process along the coordinate  $z$  can be described as follows [17]:

$$\frac{dm_s}{dz} = \frac{1}{c/n} D m_p (m_s + 1), \quad (1)$$

where  $m_s$  and  $m_p$  are the mean number of photons per mode in the laser radiation in the Raman field and pump field, respectively, and  $D$  is a proportionality constant that depends on the medium properties. The two limits of interest are described by  $m_s \ll 1$  corresponding to spontaneous Raman and  $m_s \gg 1$  corresponding to stimulated Raman scattering. In these limits, Eq. (1) yields an approximate solution for spontaneous Raman as follows:

$$m_s(z) = m_s(0) + \frac{1}{c/n} D m_p z, \quad (2)$$

where the spontaneous Raman signal depends linearly on the number of photons in the pump field  $m_p$  and the optical path in the medium  $z$ . In the case of stimulated Raman, where  $m_s \gg 1$ , the expression becomes

$$m_s(z) = m_s(0) \exp\left[\frac{D m_p z}{c/n}\right]. \quad (3)$$

The exponential dependence on pump and gain medium length for the stimulated process clearly indicates enhanced Raman scattering when condition  $m_s \gg 1$  is met.

FSRS [18–20] has been developed to implement Raman spectroscopy in a general way. The method relies on a narrow bandwidth picosecond pump and a broadband femtosecond probe pulse to stimulate the Raman process.

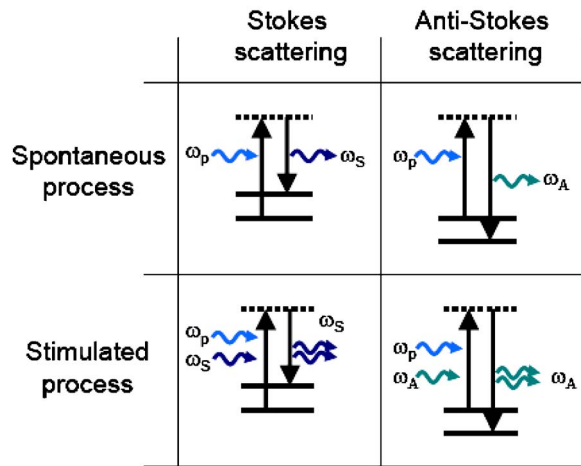


Fig. 1. (Color online) Energy diagrams describing Raman scattering. The first column depicts Stokes scattering, where the emitted photon has lower energy than the incident one. The second column depicts anti-Stokes scattering, where the emitted photon energy has higher energy than the incident one. The rows present the spontaneous and the stimulated processes, where in the case of stimulated emission, an incident field of frequency  $\omega_S$  or  $\omega_A$  triggers the transition from the virtual level to the final state of the molecule by converting  $\omega_p$  to  $\omega_S$ , or  $\omega_A$ , respectively.

Variations of the method include the collinear [20] and noncollinear geometry [21,22] of the pump and supercontinuum (SC) probe beam as well as use of the fundamental Ti:sapphire femtosecond laser system [23], the pump pulse with the modified central wavelength through frequency doubling [24], or a nonlinear parametric process [25]. The noncollinear alignment relaxes the necessity for spectral filtering of the pump beam radiation, which

would otherwise saturate the detector in the spectrometer. In the case of a Ti:sapphire amplifier where intense 800 nm pulses are available, Stokes transitions pumped by a 400 nm UV pulse (doubled, 800 nm) may be stimulated by the SC in a spectral region that has a relatively flat phase and amplitude. This allows a stimulated Raman signal to be more easily discriminated. An example of an elaborate setup with a narrow bandwidth, second-harmonic (SH) pump and noncollinear geometry is presented in the work of Laimgruber *et al.* [25].

In this paper we present a simple optical method for FSRs measurements for two liquids, acetone and methanol. We demonstrate that the temporal overlap of the SH pump and the broadband continuum induces orders-of-magnitude signal enhancement in comparison with other stimulated Raman experiments presented in the literature to date. The signal generated in this manner is the most pronounced feature of the spectra, so there is no need for further signal processing to extract the Raman peaks.

## 2. EXPERIMENTAL SETUP

The setup used for this experiment, presented in Fig. 2, is based on the construction of a noncollinear optical parametric amplifier (NOPA) [26], where a liquid sample replaces a nonlinear crystal. The source of the femtosecond pulses is a regenerative amplifier seeded by a 20 fs oscillator. The system delivers 70 fs pulses with an energy of 2.4 mJ centered at 790 nm. The amplified laser beam was first split by a fused silica plate, as shown in Fig. 2. The transmitted beam, containing most of the energy, is used for SH generation, and the reflected part is used to create the SC.

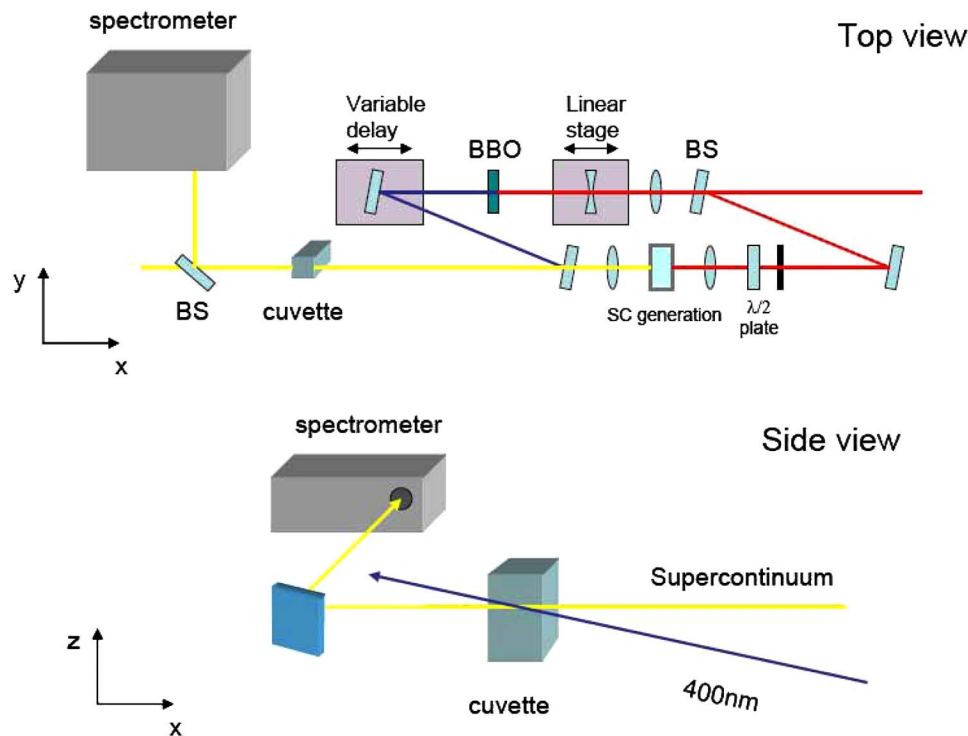


Fig. 2. (Color online) Experimental setup. The top view shows the beam path, where a small fraction of light is sent by a beam splitter (BS) through the SC arm, and the remainder is used to generate the SH, used as the Raman pump. The noncollinear geometry of the SC and the pump beams can be seen in the side view of the figure.

The 800 nm beam is recollimated by a set of two lenses,  $f=200$  mm and  $f=-100$  mm. The diverging lens is mounted on a translation stage. The telescope is set to reduce the beam diameter by a factor of 2 to increase the efficiency of frequency doubling in the beta barium borate (BBO) crystal and at the same to allow control of the intensity of our SH pump in the sample by adjustment of the lens position. The BBO crystal used for doubling is 6 mm long, and the phase-matching conditions for this long crystal results in pulses with bandwidth of  $60\text{ cm}^{-1}$ . This leads to significantly increased spectral resolution of this experiment in comparison with the alternative of using a broadband fundamental pulse ( $\sim 1500\text{ cm}^{-1}$ ). After frequency doubling, the remaining fundamental pulse is filtered from the beam by use of two mirrors designed to reflect 400 nm. The first of those mirrors is mounted on a translation stage whose motion is equivalent to changing the relative delay between the SH and SC pulses. A beam-steering mirror directs the SH onto the sample at a small angle to the plane parallel to the table. The SH pulses are  $300\text{ }\mu\text{J}$  at the sample. Since the SH is created in a Type I phase-matching process, the 400 nm polarization is perpendicular to the fundamental beam. Therefore, the polarization of the weak beam used for SC is rotated by a half-wave plate to match the SH polarization for efficient stimulation of Stokes transition. An iris is used to control the intensity of the beam, which is focused into the water cell by a lens with the focal length equal to 100 mm. The resulting SC is refocused into the sample by a  $f=50$  mm lens with energy typically less than  $10\text{ }\mu\text{J}$ . After optimizing the spatial and temporal alignment of SH and SC, a small portion of the SC is reflected by a wedged fused-silica plate, collimated, attenuated by neutral density filters, and measured by a spectrometer. The use of this type of nonlinear geometry allows direct measurement of the stimulated Raman by SC without the need to eliminate the intense SH beam in the spectrometer (for example, by use of spectral filtering).

### 3. RESULTS

Measurements were performed on two liquids, methanol having two strong Raman-active vibrations at  $2836\text{ cm}^{-1}$  and  $2945\text{ cm}^{-1}$ , and acetone with a Raman-active vibration at  $2921\text{ cm}^{-1}$ . The spectra for the 10 mm optical path with sample contained in a cuvette are presented for acetone and methanol in Figs. 3 and 4, respectively. The lighter curve shows the case of the SC overlapped in time with the SH pump and the darker curve corresponds to a reference where the pulses are temporally separated by a few ps. In both the methanol and acetone experiments, the Raman peak is the most pronounced feature of spectra. There is no need for further data enhancement such as dividing the signal by the reference, as the Raman feature is strong enough to be visually seen on a paper screen.

The acetone Raman peak is centered at  $22,033\text{ cm}^{-1}$  with FWHM of  $180\text{ cm}^{-1}$ , and this value is in good agreement with theoretical value of  $21,951\text{ cm}^{-1}$  calculated from the pump-beam central wavelength at  $24,872\text{ cm}^{-1}$ . The line width of the  $22,033\text{ cm}^{-1}$  peak is approximately three times broader than the pump-beam line width of  $\sim 60\text{ cm}^{-1}$ .

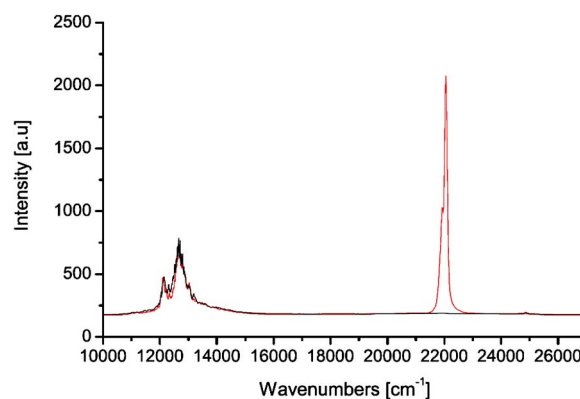


Fig. 3. (Color online) Raman spectra measured for liquid acetone using a 10 mm long sample path length. The darker curve corresponds to the spectrum recorded for SH pump and SC probe pulses temporally separated by 2 ps, and the lighter curve shows the spectrum when both pulses coincide in the acetone samples. The optimal pump beam intensity at the sample was approximately  $2 \times 10^{11}\text{ W/cm}^2$ .

The intensity of the pump and probe pulses is important for determining the mechanism contributing to the measured line shape. The contribution of the SC to broadening is minimal and can be neglected for the two following reasons. The SC intensity is at least one order of magnitude lower, and most of the energy is in the IR part of the spectrum. In addition, the SC pulse is chirped, so the intense IR spectral part is separated in time from the far-less-intense optical wavelengths, which are used to stimulate the Raman transitions. Therefore, the most intense IR part of the probe is not temporally overlapped with the SH pump and does not contribute to line broadening. The diameter of the optimized pump-beam size interacting with the sample was  $d_{\text{FWHM}}=0.9\text{ mm}$ . Assuming a temporal duration of 200 fs (from the 1.2 nm FWHM of the SH pump beam and assuming transform limited pulse), we estimate an intensity of approximately  $2.3 \times 10^{11}\text{ W/cm}^2$  at the sample. Typically, the best signal is achieved just below the self-phase modulation threshold of the SH beam (which leads to spectral broadening). The Raman

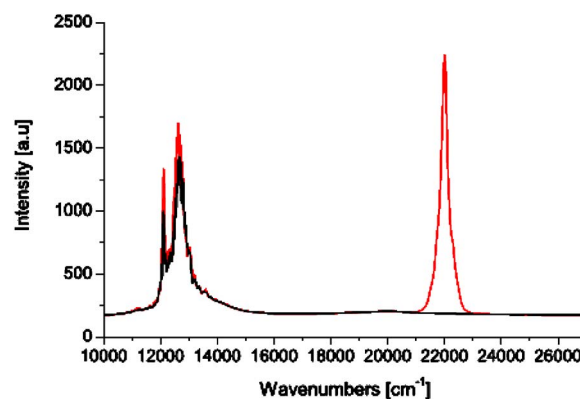


Fig. 4. (Color online) Raman spectra measured for liquid methanol using a 10 mm long sample path length. The darker curve corresponds to the spectrum recorded for SH pump and SC pulses temporally separated by 2 ps, and the lighter curve shows the spectrum when both pulses coincide in the methanol sample. The optimal pump beam intensity at the sample was approximately  $2.3 \times 10^{11}\text{ W/cm}^2$ .

transition can be stimulated by SH alone, when self-phase modulation has sufficiently broadened the SH spectrum. In this case, the stimulated Raman signal is produced along the SH beam path rather than the SC beam path. Above the self-phase modulation threshold the SH beam induces solvent boiling.

The methanol Raman peak is measured experimentally at  $21,996\text{ cm}^{-1}$  with a FWHM of  $355\text{ cm}^{-1}$ . The peak is located in between the theoretical position of the two anticipated lines at  $21,927\text{ cm}^{-1}$  and  $22,036\text{ cm}^{-1}$  corresponding to the asymmetric ( $2945\text{ cm}^{-1}$ ) and symmetric ( $2836\text{ cm}^{-1}$ ) vibrational modes, respectively. These modes could not be resolved because the bandwidth of the SH is in the order of the separation of those lines.

The measurements were repeated with an optical path decreased to 1 mm and with the pump beam size at the sample adjusted for the optimal signal. The optimal beam diameter of the SH pump differs slightly for both investigated liquids. In the case of acetone, the FWHM of the transverse laser beam profile was approximately 0.65 mm, and in the methanol study the FWHM beam diameter was 0.62 mm. These correspond to intensities at the sample of approximately  $4.5 \cdot 10^{11}\text{ W/cm}^2$  and  $4.9 \cdot 10^{11}\text{ W/cm}^2$  for acetone and methanol, respectively. The different intensities can be explained by a higher nonlinear index of refraction  $n_2$  for acetone than for methanol. The  $n_2$  is responsible for the self-phase modulation and the self-focusing of the pump beam. The magnitude of the  $n_2$  sets the intensity limit when undesired nonlinear effects distort the pump spatially and spectrally, leading to self-focusing, beam collapse and solvent boiling. The difference in the pump beam diameter is not measurable in case of 10 mm samples of those two fluids, since the intensities were 2–2.5 times lower and the effect of the intensity-dependent index of refraction was less pronounced. The Raman signal is still clearly visible, as shown in Figs. 5 and 6. The relative peak amplitude has changed significantly in comparison to the 10 mm case. The peak intensity is much lower and has increased width and nonuniform structure.

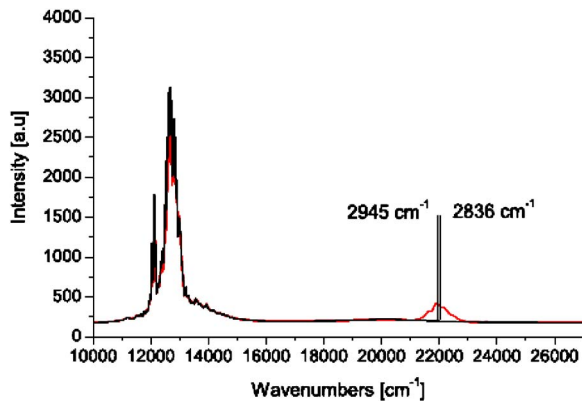


Fig. 5. (Color online) Methanol Raman spectra measured for the 1 mm long sample path length. The darker curve corresponds to the spectrum recorded for SH pump and SC probe pulses temporally separated by 2 ps, and the lighter curve shows the spectrum when both pulses coincide in time. The vertical lines mark the positions of the anticipated Raman lines. The optimal beam intensity at the sample was approximately  $4.9 \cdot 10^{11}\text{ W/cm}^2$ .

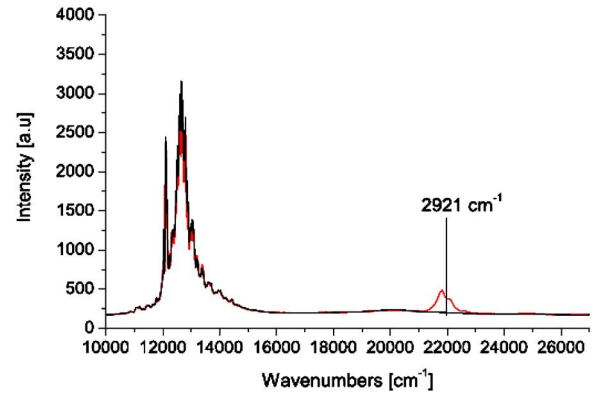


Fig. 6. (Color online) Acetone Raman spectra measured for the 1 mm long sample path length. The darker curve corresponds to the spectrum recorded for SH pump and SC probe pulses temporally separated by 2 ps, and the lighter curve shows the spectrum when both pulses coincide in time. The vertical line marks the position of the anticipated Raman line. The optimal beam intensity at the sample was approximately  $4.5 \cdot 10^{11}\text{ W/cm}^2$ .

The lower Raman peak intensity for the case of the 1 mm path-length experiment can be explained by the optimal pump intensity combined with the optical path length when compared with those parameters for the 10 mm case. The gain factor in Eq. (3),  $(\exp[2Dm_p/c/nz])$ , predicts an exponential rise of the signal with increased laser intensity ( $\sim m_p$ ) and necessary propagation length  $z$ . The 10-times-shorter optical path in the medium can not be counterbalanced by higher intensity (to maintain the same gain) because of the undesirable effects arising from the intensity-dependent index of refraction. Those effects limit the maximum intensity for the 1 mm case to below the one required to balance the shorter optical path. With higher pump-beam intensity, self-phase modulation will generate additional bandwidth and induce a stimulated Raman signal along the pump-beam path rather than along the SC path. When the pump-beam intensity is increased even further, solvent boiling and beam breakup will occur due to the self-focusing.

Another important feature of the observed peaks in the 1 mm path-length experiment is their increased spectral width. For methanol the width has changed from  $355\text{ cm}^{-1}$  for 10 mm sample to  $620\text{ cm}^{-1}$  for 1 mm sample, and for acetone the corresponding widths increased from  $180\text{ cm}^{-1}$  to  $470\text{ cm}^{-1}$ . This broadening is very likely due to cross-phase modulation induced by the strong pump. In cross-phase modulation the temporal intensity profile modifies the index of refraction of the medium. This modulates the phase experienced by the weak, stimulated Raman pulse during temporal overlap with the pump beam and, as in the case of self-phase modulation, leads to spectral broadening of the weak beam. The process can be described by considering the intensity driving the change of the nonlinear index of refraction in time:

$$n(t) = n_0 + n_2 I(t), \quad (4)$$

which modifies the temporal phase of the pulse:

$$\Phi(t) = \omega_0 t + kzn(t), \quad (5)$$

and that leads to the change in instantaneous frequency defined as

$$\omega_i(t) = \frac{\partial \Phi(t)}{\partial t}. \quad (6)$$

Assuming the Gaussian temporal envelope of the pulse, the maximum frequency shift  $\Delta\omega$  is described by the proportionality

$$\Delta\omega \propto \frac{I_0 n_2 z}{\tau_p^2}, \quad (7)$$

where  $I_0$ ,  $\tau_p$ ,  $n_2$ , and  $z$  represent the intensity, pulse duration, nonlinear index of refraction, and optical path in the medium, respectively. The above analysis does not include dispersion, so we do not expect accurate results for the longer-length samples where the temporal envelope will evolve in time. For the 1 mm sample, where the pulse duration does not change significantly, the maximum broadening calculated using  $n_2 = 24 * 10^{-16} \text{ cm}^2/\text{W}$  [27] and the upper estimate for intensity for the acetone is  $1285 \text{ cm}^{-1}$ , whereas the experimentally measured FWHM of the peak was  $470 \text{ cm}^{-1}$ . In the case of methanol there are two lines separated by  $109 \text{ cm}^{-1}$ , and since it is below the resolution of our experiment, we observe the peak with the width of  $620 \text{ cm}^{-1}$ . The calculated frequency broadening using  $n_2 = 7 * 10^{-16} \text{ cm}^2/\text{W}$  [27] is  $408 \text{ cm}^{-1}$ , so considering the two lines gives a theoretical width of  $517 \text{ cm}^{-1}$ , which is in good agreement with the measured value. For the 10 mm samples, on the other hand, the calculated broadening is unrealistically large, but the model does not include dispersion and assumes that the pulse will propagate through the sample without any change in the envelope. In a 10 mm sample the pulse will change because of dispersion, so more elaborate numerical simulation will be necessary to include all the relevant effects. We propose that in case of longer length samples, where the intensity of the pump pulse is significantly lower, dispersion acts before nonlinear effects, extends the pump-pulse duration, and therefore reduces the cross-phase modulation of the Raman signal.

One interesting point raised by these measurements concerns whether or not remote detection based on a stimulated Raman can be realized in the gas phase. This question is of particular interest in the field of remote sensing and detection. Given the density of the 1 mm length of the liquid sample we calculate a corresponding optical path of approximately 140 cm in the gas phase for acetone and 470 cm for methanol at standard temperature and pressure. For lidar-like remote detection [28], a collinear configuration seems to be much more feasible and attractive with the filamentation in the atmosphere as a SC source. In such configuration the interaction length would be rather limited by the walk-off of the pump pulse from the Stokes pulse due to the air dispersion. In the case of air dispersion, the group velocity mismatch for SH and Stokes pulse is  $\sim 26 \text{ fs/m}$ . Thus for 200 fs pulses, the distance from where the pulses just precede to overlap (through exact overlap) to being out of overlap would be on the order of 15 m. Since the SC is known to have linear chirp in the visible part of the spectrum, the difference in group velocity dispersion for specific spectral components of the SC corresponding to Raman transition and the pump beam might be used to our

advantage. By properly choosing the relative delay between the SC and SH beams, their overlap is achieved at the predefined spatial coordinates, which we anticipate would make a very useful contribution to remote detection of molecular species.

## 4. CONCLUSIONS

We have presented a method that induces an exceptionally strong Raman signal from liquid samples of acetone and methanol by use of a noncollinear UV pump and a SC stimulating beam alignment. In our optical design the Raman transition is stimulated using a nearly flat spectral phase and amplitude seed pulse in the visible region of a SC, with the pump operating at the SH (400 nm) of the fundamental wavelength of a Ti:sapphire amplifier system. The choice of the pump beam in the visible, rather than the near infrared, offers the advantage of observing the Stokes transition without interference from self-phase modulation features in the SC. The noncollinear geometry employed gives much higher dynamical range for the Raman signal, since the strong pump beam is spatially separated and does not enter the spectrometer. This allows detection of the relatively weak SC, exclusively. Finally, we presented calculations of the self-phase modulation effects lowering the resolution of the spectra and at the same time limiting the maximum yield of the stimulated Raman process.

## ACKNOWLEDGMENTS

The authors gratefully acknowledge financial support from the United States Army Research Office (USARO) and the DoD MURI program as administered by the U. S. Army Research Office.

## REFERENCES

1. K. Uehara and H. Tai, "Remote detection of methane with a 1.66  $\mu\text{m}$  diode laser," *Appl. Opt.* **31**, 809–814 (1992).
2. T. Henningsen, M. Garbuny, and R. L. Byer, "Remote detection of CO by parametric tunable laser," *Appl. Phys. Lett.* **24**, 242–244 (2003).
3. D. Killinger and A. Mooradian, *Optical and Laser Remote Sensing*, Vol. 39, of Springer Series in Optical Sciences (Springer-Verlag, 1983).
4. A. Mohebati and T. A. King, "Remote detection of gases by diode laser spectroscopy," *J. Mod. Opt.* **35**, 319–324 (1988).
5. J. C. Carter, S. M. Angel, M. Lawrence-Snyder, J. Scaffidi, R. E. Whipple, and J. G. Reynolds, "Standoff detection of high explosive materials at 50 meters in ambient light conditions using a small Raman instrument," *Appl. Spectrosc.* **59**, 769–775 (2005).
6. R. W. Hellwarth, "Theory of stimulated Raman scattering," *Phys. Rev.* **130**, 1850–1852 (1963).
7. G. Eckhardt, S. E. Schwarz, F. J. McClung, R. W. Hellwarth, E. J. Woodbury, and D. Weiner, "Stimulated Raman scattering from organic liquids," *Phys. Rev. Lett.* **9**, 455–457 (1962).
8. A. K. Misra, S. K. Sharma, and P. G. Lucey, "Remote Raman spectroscopic detection of minerals and organics under illuminated conditions from a distance of 10 m using a single 532 nm laser pulse," *Appl. Spectrosc.* **60**, 223–228 (2006).
9. A. K. Misra, S. K. Sharma, C. H. Chio, P. G. Lucey, and B. Lienert, "Pulsed remote Raman system for daytime

- measurements of mineral spectra," *Spectrochim. Acta, Part A* **61**, 2281–2287 (2005).
10. T. Chen, J. M. J. Madey, F. M. Price, S. K. Sharma, and B. Lienert, "Remote Raman spectra of benzene obtained from 217 meters using a single 532 nm laser pulse," *Appl. Spectrosc.* **61**, 624–629 (2007).
  11. S. K. Sharma, A. K. Misra, and B. Sharma, "Portable remote Raman system for monitoring hydrocarbon, gas hydrates and explosives in the environment," *Spectrochim. Acta, Part A* **61**, 2404–2412 (2005).
  12. B. J. Pearson, J. L. White, T. C. Weinacht, and P. H. Bucksbaum, "Coherent control using adaptive learning algorithms," *Phys. Rev. A* **63**, 063412 (2001).
  13. B. J. Pearson and P. H. Bucksbaum, "Control of Raman lasing in the nonimpulsive regime," *Phys. Rev. Lett.* **92**, 243003 (2004).
  14. T. C. Weinacht, J. L. White, and P. H. Bucksbaum, "Toward strong field mode-selective chemistry," *J. Phys. Chem. A* **103**, 10166–10168 (1999).
  15. M. Spanner and P. Brumer, "Mechanisms for the control of two-mode transient stimulated Raman scattering in liquids," *Phys. Rev. A* **73**, 023809 (2006).
  16. M. Spanner and P. Brumer, "Two-pulse control of Raman scattering in liquid methanol: the dominance of classical nonlinear optical effects," *Phys. Rev. A* **73**, 023810 (2006).
  17. R. W. Boyd, *Nonlinear Optics*, 2nd ed. (Academic Press, 2003).
  18. D. W. McCamant, P. Kukura, and R. A. Mathies, "Femtosecond broadband stimulated Raman: a new approach for high-performance vibrational spectroscopy," *Appl. Spectrosc.* **57**, 1317–1323 (2003).
  19. P. Kukura, D. W. McCamant, and R. A. Mathies, "Femtosecond stimulated Raman spectroscopy," *Anal. Chem.* **78**, 5952–5959 (2006).
  20. D. W. McCamant, P. Kukura, S. Yoon, and R. A. Mathies, "Femtosecond broadband stimulated Raman spectroscopy: apparatus and methods," *Rev. Sci. Instrum.* **75**, 4971–4980 (2004).
  21. S. M. Jin, Y. J. Lee, J. W. Yu, and S. K. Kim, "Development of femtosecond stimulated Raman spectroscopy: stimulated Raman gain via elimination of cross phase modulation," *Bull. Korean Chem. Soc.* **25**, 1829–1832 (2004).
  22. S. A. Kovalenko, A. L. Dobryakov, J. Ruthmann, and N. P. Ernsting, "Femtosecond spectroscopy of condensed phases with chirped supercontinuum probing," *Phys. Rev. A* **59**, 2369–2384 (1999).
  23. E. Ploetz, S. Laimgruber, S. Berner, W. Zinth, and P. Gilch, "Femtosecond stimulated Raman microscopy," *Appl. Phys. B* **87**, 389–393 (2007).
  24. S. Shim and R. A. Mathies, "Generation of narrow-bandwidth picosecond visible pulses from broadband femtosecond pulses for femtosecond stimulated Raman," *Appl. Phys. Lett.* **89**, 121124 (2006).
  25. S. Laimgruber, H. Schachenmayr, B. Schmidt, W. Zinth, and P. Gilch, "A femtosecond stimulated Raman spectrograph for the near ultraviolet," *Appl. Phys. B* **85**, 557–564 (2006).
  26. J. Piel, E. Riedle, L. Gundlach, R. Ernstorfer, and R. Eichberger, "Sub-20 fs visible pulses with 750 nJ energy from a 100 kHz nonco-linear optical parametric amplifier," *Opt. Lett.* **31**, 1289–1291 (2006).
  27. P. E. Ciddor, "Refractive index of air: new equations for the visible and near infrared," *Appl. Opt.* **35**, 1566–1573 (1996).
  28. K. Stelmaszczyk, P. Rohwetter, G. Mejean, J. Yu, E. Salmon, J. Kasparian, R. Ackermann, J.-P. Wolf, and L. Woste, "Long-distance remote laser-induced breakdown spectroscopy using filamentation in air," *Appl. Phys. Lett.* **85**, 3977–3979 (2004).